ADVANCES IN ATMOSPHERIC SCIENCES, VOL. 31, MARCH 2014, 252–262

Can Adaptive Observations Improve Tropical Cyclone Intensity Forecasts?

QIN Xiaohao*[1] and MU Mu[2]

[1]*State Key Laboratory of Numerical Modeling for Atmospheric Sciences and Geophysical Fluid Dynamics, Institute of Atmospheric Physics, Chinese Academy of Sciences, Beijing* 100029

[2]*Key Laboratory of Ocean Circulation and Waves, Institute of Oceanology, Chinese Academy of Sciences, Qingdao* 266071

(Received 12 January 2013; revised 22 May 2013; accepted 19 June 2013)

ABSTRACT

In order to investigate whether adaptive observations can improve tropical cyclone (TC) intensity forecasts, observing system simulation experiments (OSSEs) were conducted for 20 TC cases originating in the western North Pacific during the 2010 season according to the conditional nonlinear optimal perturbation (CNOP) sensitivity, using the fifth version of the PSU/NCAR mesoscale model (MM5) and its 3DVAR assimilation system. A new intensity index was defined as the sum of the number of grid points within an allocated square centered at the corresponding forecast TC central position, that satisfy constraints associated with the Sea Level Pressure (SLP), near-surface horizontal wind speed, and accumulated convective precipitation. The higher the index value is, the more intense the TC is.

The impacts of the CNOP sensitivity on the intensity forecast were then estimated. The OSSE results showed that for 15 of the 20 cases there were improvements, with reductions of forecast errors in the range of 0.12%–8.59%, which were much less than in track forecasts. The indication, therefore, is that the CNOP sensitivity has a generally positive effect on TC intensity forecasts, but only to a certain degree. We conclude that factors such as the use of a coupled model, or better initialization of the TC vortex, are more important for an accurate TC intensity forecast.

Key words: adaptive observation, tropical cyclone, intensity forecast, conditional nonlinear optimal perturbation

Citation: Qin, X. H., and M. Mu, 2014: Can adaptive observations improve tropical cyclone intensity forecasts? *Adv. Atmos. Sci.*, **31**(2), 252–262, doi: 10.1007/s00376-013-3008-0.

1. Introduction

As severe natural disasters, tropical cyclones (TCs) cause huge human and economic losses every year. Hence, accurate TC forecasts in areas threatened by such storms is of great importance. Since the beginning of the numerical weather forecasting era, researchers have considered many ways to obtain more accurate forecasts of both TC track and intensity, such as the application of advanced numerical models, satellite observations, and adaptive observations over the Atlantic and eastern Pacific (Aberson, 2002, 2003), and western Pacific (Wu et al., 2005, 2007; Elsberry and Harr, 2008) during the last decade. Consequently, TC track forecasts have improved significantly, and errors have been reduced by nearly 50% over the period 1980–2008 for forecasts in the Atlantic and eastern North Pacific (Franklin, 2009). The contribution of aircraft-deployed dropwindsondes used for adaptive observations has been particularly notable. Wu et al. (2007) showed that, during the first 72 h, the mean track error reductions in the National Centers for Environmental Prediction (NCEP) Global Forecast System (GFS), Fleet Numerical Meteorology and Oceanography Center (FNMOC) Navy Operational Global Atmospheric Prediction System (NOGAPS), and the Japanese Meteorological Agency (JMA) Global Spectral Model (GSM), are 14%, 14% and 19%, respectively. Statistical results from the 2003–09 Dropwindsonde Observations for Typhoon Surveillance near the Taiwan Region (DOTSTAR) program showed that assimilation of dropwindsonde data could lead to a 60% improvement in 1- to 5-day track forecasts and a 10%–20% mean track error reduction with at least a 90% confidence level (Chou et al., 2011).

In contrast, many factors have hampered the development of TC intensity forecasting, including inaccurate initialization of the TC vortex, imperfect physical parameterization, and a lack of data regarding the inner area of TCs. Therefore, how to improve TC intensity forecasting has become a hot topic in recent times. Efforts have focused on understanding the environmental dynamical factors affecting TC intensification, intensity, and life peak intensity (Zeng et al., 2006), the effects of terrain and land surface variation on the observed evolution of the eyewall (Wang and Cheng, 2008), the inter-relationships between upper-ocean thermal structure

* Corresponding author: QIN Xiaohao
Email: xhqin@lasg.iap.ac.cn

and western North Pacific category 5 typhoons (Lin et al., 2007, 2008), concentric sensitivity of the simulated TC inner-core size to the initial vortex size (Xu and Wang, 2010), eye-wall formation (Wu et al., 2011), and the assimilation of airborne radar observations through an ensemble Kalman filter (Weng and Zhang, 2012). The combined impact of such studies will be to improve the accuracy of TC intensity forecasts in the near future.

Qin and Mu (2011b) evaluated the influence of the conditional nonlinear optimal perturbation (CNOP) sensitivity on TC track forecasts by assimilating simulated dropwindsonde observational data. The CNOP sensitivity had an average positive effect on the TC track forecasts. In addition, the CNOP sensitivity generally performed better than the sensitivities of the five leading singular vectors (SVs) (Palmer et al., 1998). Hence, CNOP is an effective method to identify sensitive regions for TC adaptive observations. The general beneficial effects of adaptive observations on TC track forecasting established from such research motivated us to investigate whether its impacts on TC intensity forecasts would also be positive. This is the question we aim to answer in the present paper.

The remainder of the paper is organized as follows. Section 2 describes the method, model and strategy used in the study. Section 3 details the TC intensity index, which embodies the synthetic impacts of sea level pressure (SLP), near-surface horizontal wind speed (WIND), and accumulated convective precipitation (PP). Section 4 considers the influence on TC intensity forecasts of assimilating simulated dropwindsonde data deployed in sensitive regions identified by CNOP. Finally, conclusions and a discussion are presented in section 5.

2. Method, model and strategy

As a method to identify sensitive regions in adaptive observations, CNOP has been successfully applied in many published studies (Mu et al., 2009; Wang and Tan, 2009; Wang et al., 2011; Qin and Mu, 2011a, 2011b; Zhou and Mu, 2011, 2012a, 2012b; Chen and Mu, 2012; Chen et al., 2013; Qin et al., 2013). Using similar mathematic principles, CNOP has also been employed in the predictability of ENSO (Duan et al., 2004; Mu et al., 2007; Duan et al., 2009; Yu et al., 2009; Duan and Luo, 2010; Yu et al., 2012a, 2012b;), thermohaline circulation (Mu et al., 2004; Sun et al., 2005), blocking events (Jiang and Wang, 2010; Jiang and Wang, 2011; Mu and Jiang, 2011), simulation and predictability of ecosystems (Sun and Mu, 2009; Sun et al., 2010; Sun and Mu, 2011, 2012), and cold vortices (Jiang and Wang, 2011).

The same structure and computation of CNOP as in Qin et al. (2013) was used in the present study. CNOP (δX_0^*) is the initial perturbation (δX_0), superimposed to initial analysis (X_0), whose nonlinear evolution (using nonlinear model M) attains the maximal value of the cost function J at verification time t (Mu et al., 2003; Mu and Zhang, 2006) for a chosen norm $\|\cdot\|$:

$$J(\delta X_0^*) = \max_{\|\delta X_0\| \leqslant \beta} \|M(X_0 + \delta X_0) - M(X_0)\|. \qquad (1)$$

Here, $\|\delta X_0\| \leqslant \beta$ is the initial constraint defined by the chosen norm $\|\cdot\|$, which reflects the physical laws that the initial perturbation should satisfy. This norm also measured the evolution of the initial perturbations in the present study. In predictability studies, CNOP represents the initial error that has the worst impacts on the prediction result at verification time (Mu et al., 2003). Especially for TC events, CNOP can be used to identify the initial error that causes the largest prediction error (Mu et al., 2009). Consequently, the worst forecast would be avoided if the CNOP is eliminated in the initial analysis.

The CNOP calculated in the present study optimized the perturbation energy evolution over a 48-hr optimization period employing adjoint models of the fifth version of the Pennsylvania State University/National Center for Atmospheric Research (PSU/NCAR) mesoscale model (MM5) based on the ERA-Interim reanalysis from the European Centre for Medium-Range Weather Forecasts (ECMWF). The physical parameterizations used in the simulation included the dry convective adjustment scheme, the grid-resolved large-scale precipitation scheme, the high-resolution PBL scheme, and the Kuo cumulus parameterization scheme. The horizontal area covered a 121(lat) $\times$ 81(lon) square lattice with a horizontal resolution of 60 km and 11 levels in the vertical direction, with the top level at 50 hPa. The verification region was approximately a 15° (lat) $\times$12° (lon) box centred at the central forecast position of the corresponding TC at 48 h (verification time).

We used the total dry energy norm (G_{de}) to measure the initial perturbations and the evolution of the perturbations, which can be expressed as

$$G_{\mathrm{de}}(\delta X_0) = \frac{1}{D}\int_D \int_0^1 \left[u_0'^2 + v_0'^2 + \frac{c_p}{T_{\mathrm{r}}} T_0'^2 + R_{\mathrm{a}} T_{\mathrm{r}} \left(\frac{p_s'}{p_{\mathrm{r}}} \right)^2 \right] \mathrm{d}\sigma \mathrm{d}s\,, \qquad (2)$$

where D is the horizontal model region; σ is the vertical coordinate; $c_p = 1005.7$ J kg^{-1} K^{-1}, which is the specific heat at constant pressure; $R_{\mathrm{a}} = 287.04$ J kg^{-1} K^{-1}, which is the dry air constant; $p_{\mathrm{r}} = 1000$ hPa; and $T_{\mathrm{r}} = 270$ K. δX_0 is composed of u_0', v_0', T_0' and p_s', which are the perturbed zonal and meridional wind components, temperature and surface pressure, respectively. The integration extends over the full domain D and the vertical direction σ. According to Eq. (2), CNOP sensitivity comprises the grids with larger perturbation energy.

After identifying CNOP sensitivity, we conducted observing system simulation experiments (OSSEs) in these regions for each individual case to estimate the impacts of CNOP sensitivity on TC intensity forecasts. The forecasts from 0 up to 48 h initiated with the NCEP reanalysis data were deemed as the "truth", and during that period, TC

forecast intensity was specified at 6-h intervals to represent the "true" situation. In order to estimate the statistics of the OSSE truth run to reality, we compared the simulated TC centers in the OSSE truth run with best track data from the Joint Typhoon Warning Center (JTWC). We found that, on average for all 20 cases, the difference increased monotonically as the forecast period increased, from being 92.4 km at 12 h to 325.9 km at 48 h. The simulation within 24 h of the OSSE truth run had comparative track forecast errors with those of the National Hurricane Center (NHC) for Atlantic basin tropical storms and hurricanes from 2000 to 2009. However, the track forecast errors of the OSSE truth run over 30 h were larger—albeit not too much larger—than those of the NHC from 2000 to 2009. Generally, the track forecast errors of the OSSE truth run in the present study were acceptable. Forecasts during the same period, but initiated with the ERA-Interim reanalysis from the ECMWF, represented the control run situation. The differences between the TC intensities of the control run and the truth run were defined as the TC intensity forecast error without dropwindsonde data, which only came from using different initial reanalysis data. Simultaneously, 15 sets of simulated observation data, including temperature, horizontal wind speed, and horizontal wind direction at 850, 500 and 200 hPa, which were the sum of the forecasts of the truth run at initial time and Gaussian distribution perturbations with zero expectation and different standard deviations (order of 10^{-1} of the analysis) according to different variables, were obtained by dropwindsondes over CNOP sensitivity. These dropwindsonde data were then assimilated by the 3DVAR assimilation system of MM5 to produce an analysis at 0 h, which could then be used to predict the TC intensities during the following 48 h. The differences between this TC intensity and the truth run were defined as the TC intensity forecast errors with dropwindsondes. Differences between these errors and those without could indicate the influence of CNOP sensitivity on TC intensity forecasts.

TC cases that originated in the western North Pacific during the 2010 season were examined. In total, there were 14 TCs in that year according to the China Meteorological Administration (CMA). However, for one TC [Namtheum (2010)], the lifetime was shorter than 48 h, which is the optimization period needed for CNOP calculation; and for two others [Kompasu (2010) and Mindulle (2010)], the vortex structure of was not simulated well by the model. Furthermore, where the lifetime of a TC was longer than 96 h, it was separated into two continuous cases. Hence, the remaining 11 TCs were separated into 20 cases according to their lifetimes, and these formed the research objects of the study.

3. TC intensity index

Instead of using the conventional definition that relies on only the SLP or maximum horizontal wind, we have defined a new index that gives a direct snapshot of the degree of potential impact of a TC, and one that could help the public to determine their activities in the following hours. In this section, we first detail this new TC intensity index and compare it with the conventional definition, and then we specify the TC intensity forecast error in the OSSEs.

3.1. *Definition*

In order to estimate, conveniently and quantitatively, the impacts of a TC within a limited region, we first allocate a square centered at the forecasted central position at specified times (from 12 h to 48 h at 6-h intervals) and with a side length of 720 km. Because the horizontal spacing between model grid points is 60 km, there are 169 grid points within this square. At each grid point, information about three TC variables is considered in forming the TC intensity index: the SLP, WIND at 925 hPa, and 12-h PP. We choose three CMA criteria as references and thus use 1010 hPa (tropical depression), 15.2 m s^{-1} (level 7), and 5 mm (a medium amount of rain) to represent the respective limits for SLP, WIND at 925 hPa, and 12-h PP. These thresholds are determined by iterative tests to satisfy the following two criteria: to reflect the simulation ability of the model itself; and to be enough to represent the impact of a TC. We count the grid points where each separate criterion is satisfied. The TC intensity index is then defined to be the sum of the three counts. For example, if the number of grid points with SLP lower than 1010 hPa (or WIND at 925 hPa larger than 15.2 m s^{-1} or 12-h PP greater than 5 mm) is A (or B or C), then the index equals A+B+C. That is, this index considers a synthetic impact of a TC within this square according to three factors. The higher the index value is, the more intense the TC is.

We compared the new index measuring TC intensity with the conventional one that relies on the maximum near-surface wind speed. By using the maximum wind speed at every 6-h interval, each TC case was classified as a (super) typhoon, severe tropical storm, tropical storm, or tropical depression (colors in Fig. 1). We then identified the TC intensity at every 6-h interval according to our index (y-axis in Fig. 1). Generally, the index changes synchronously with the maximum wind speed. It ranges between 300 and 400 when the maximum wind speed is in the typhoon or super typhoon category. If a TC case remains in the tropical depression category during most of the 36 h, the index falls into 100–200. The (severe) tropical storms are positioned between the above two cases. A similar comparison was performed according to the central SLP, and the results were consistent with those according to the maximum near-surface wind speed (data not shown).

Therefore, the index used in the present study is generally in line with the conventional definition of TC intensity, but possesses a number of advantages. Suppose there are two TC cases in the same location with the same maximum wind speed of 45 m s^{-1}. With respect to the conventional definition, the intensity of these two TCs is the same. However, the degree of their impacts could be different. Is it just limited to a small region, or does it influence a large area? If reporting is based only on the conventional definition, the public does not receive detailed information about the degree to which they will be affected by an approaching TC. Instead, the new in-

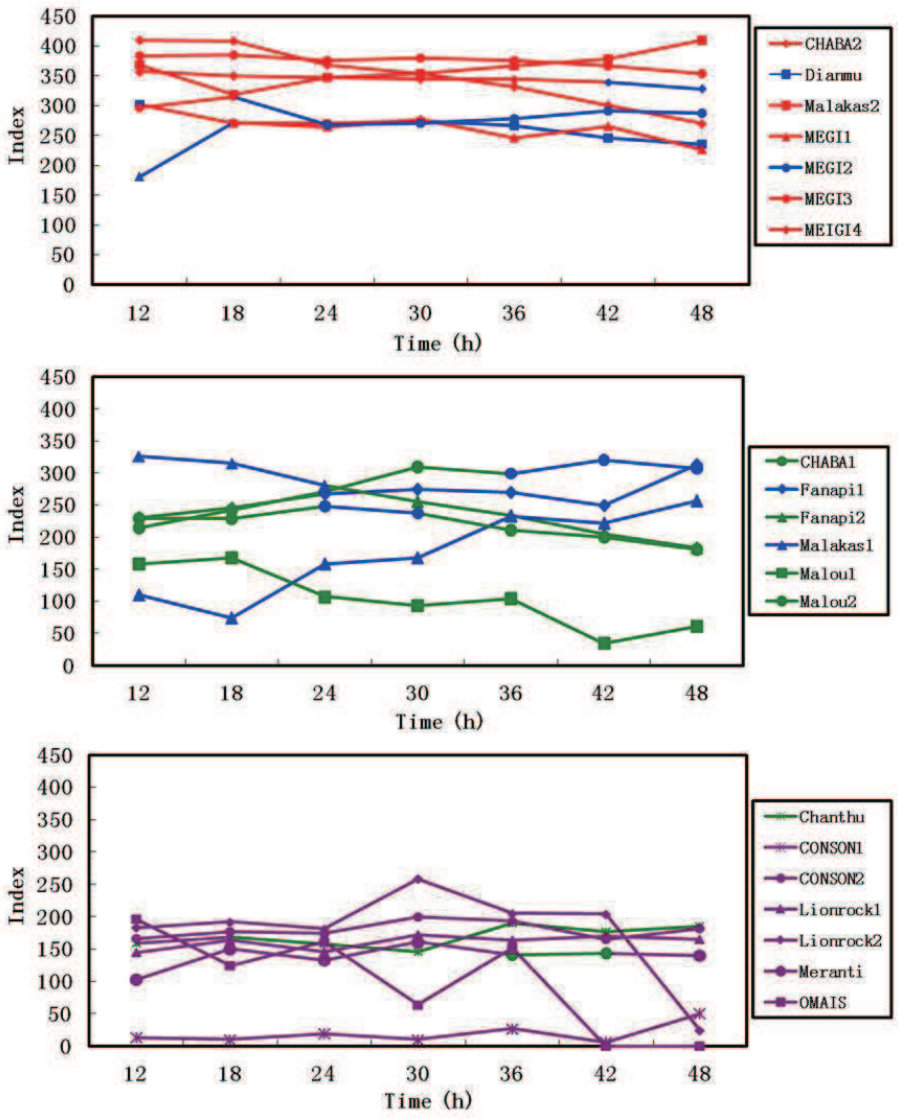

Fig. 1. TC intensity index for all 20 cases during the period 12–48 h at 6-h intervals. Red, blue, green and purple lines represent (super) typhoons, severe tropical storms, tropical storms and tropical depressions, respectively, according to the conventional intensity definition that relies on maximum horizontal wind speed.

tensity index used in the present study provides a direct snapshot about the potential degree of impact of a TC, and could help the public to determine their activities in the following hours.

3.2. *TC intensity forecast error in the OSSEs*

To quantitatively estimate the impacts of the CNOP sensitivity on TC intensity forecasts, we specify the TC intensity forecast error in the OSSEs. As discussed in the previous section, the TC intensity index consists of three variables (A, B, and C) and represents the number of grid points satisfying the conditions of SLP, WIND and PP, respectively. The letters A, B and C are used for the truth run; for the control (OSSE) run, the corresponding values are denoted by a, b and c. The definition of the TC intensity forecast error (IFE) is

$$(|A-a|+|B-b|+|C-c|)\times\frac{100}{A+B+C}\%\,. \qquad (3)$$

The IFE represents the difference in intensity between the control (OSSE) and truth runs in the allocated square. If the IFE equals zero, this means that the forecast intensity in the corresponding control (OSSE) run is the same as that in the truth run, suggesting there is no intensity forecast error between them. The larger the IFE is, the larger the intensity forecast error is, indicating that the intensity predicted by the control (OSSE) becomes increasingly different from the true state. We calculated the IFE twice at every 6-h interval during the period 12–48 h for each TC case, to represent the

cases with and without dropwindsonde data. The differences between the cases illustrate the influence of the CNOP sensitivity on the TC intensity forecast.

4. OSSE results and case analyses

The IFE at intervals of 6 h during the period 12–48 h for each TC case are shown in Fig. 2. In each plot, two groups of bars represent the IFE in Eq. (3) at different times beginning from 12 h. Generally, IFEs with dropwindsonde data were lower than those without dropwindsonde data in 15 of the 20 cases, and there was a mean reduction in error of 0.12%–8.59% for the period 12–48 h. In contrast, five cases showed increased forecast errors of 0.20%–18.37% after utilizing the dropwindsonde data. In some cases, including CONSON1 (2010), Fanapi1 (2010), MEGI3 (2010), CHABA1 (2010) and CHABA2 (2010), the level of improvement after using dropwindsonde data was marked. However, in the Malou1 (2010) case, the use of dropwindsonde data caused the intensity forecast to be completely different from the true state, and resulted in the worst forecast among all the 20 cases (the IFE increased by 18.37%). For nearly half of the 20 cases, the average changes before and after assimilation of dropwindsonde data were not that remarkable. On some occasions, the differences between control and OSSE at each individual time point were quite major. However, for half of the time points from 12 to 48 h, the changes were positive (reduced errors), and for the other half the changes were negative (increased errors). Overall, these two opposing sets of results culminated in an almost neutral effect [e.g.,

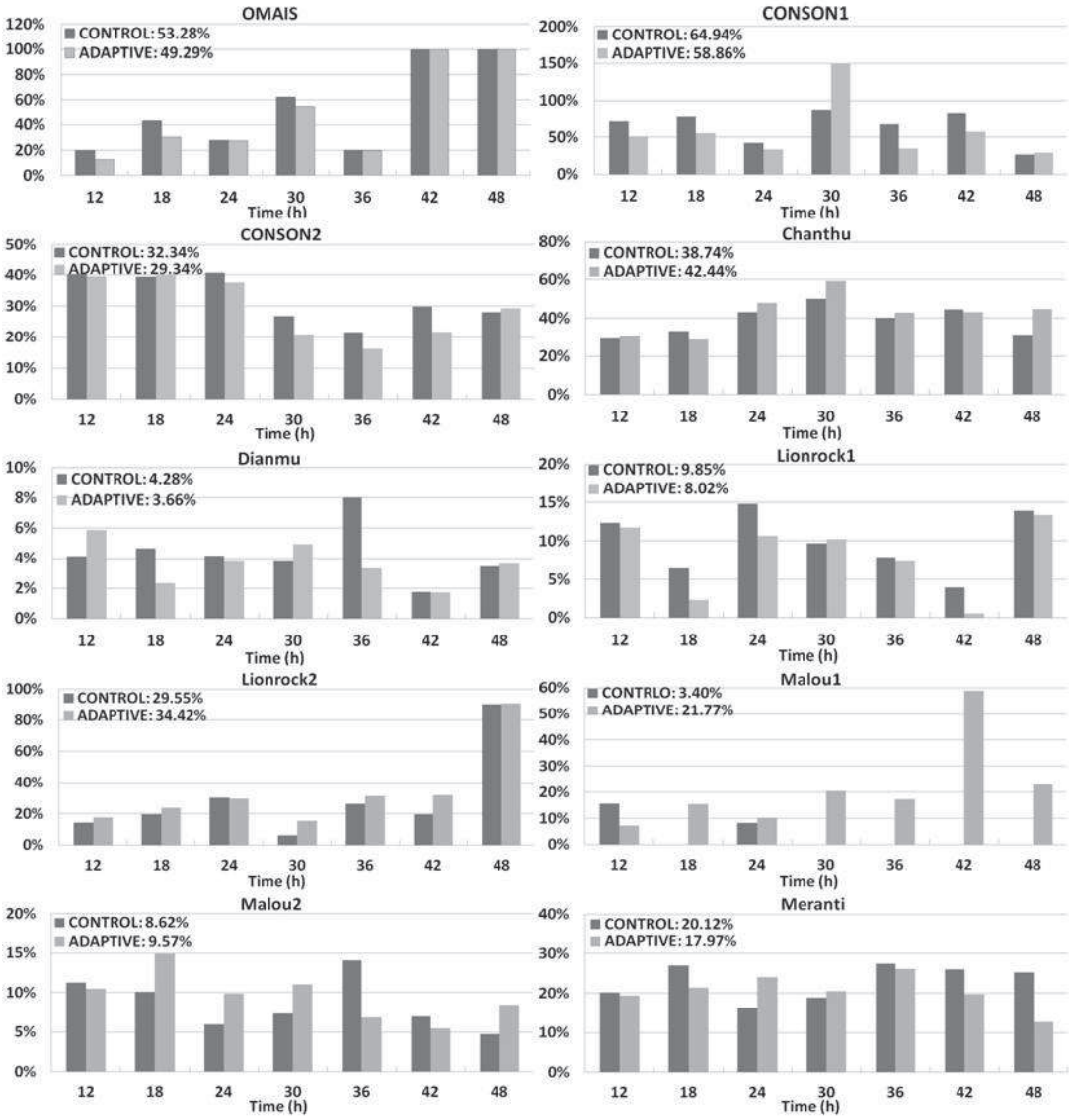

Fig. 2. Intensity forecast errors (IFE) for the 20 cases without (black bars) and with (gray bars) dropwindsondes during the 12–48-h period. The numbers included in the upper left of each panel indicate the average forecast errors during the period.

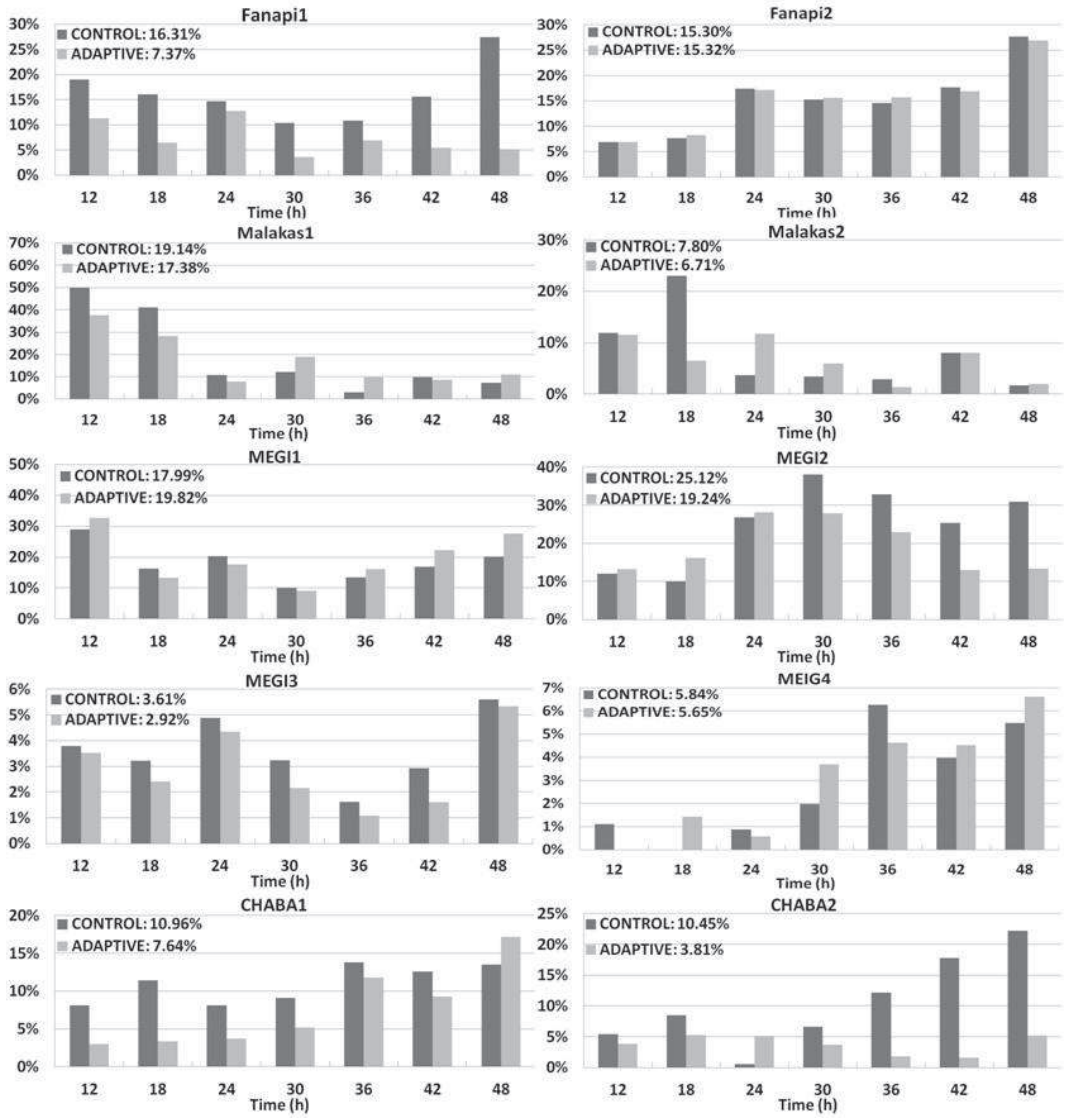

Fig. 2. (continued.)

Malakas2 (2010)]. On other occasions, the intensity forecasts with and without dropwindsonde data were similar at each individual time point [e.g., Lionrock2 (2010)]. Now follows a detailed analysis of representative cases in which the inclusion of dropwindsonde data had marked effects. Cases of improvement and deterioration are both considered. No further discussion about neutral cases is provided.

Fanapi1 (2010) is a representative case of intensity forecast improvement. It remained as a tropical storm, but then intensified to a severe tropical storm during the second 24 h. The intensity forecast errors were reduced markedly in the OSSE run at all intervals from 12 h up to 48 h, although not at 24 h. The improvement in the intensity forecast at 48 h was the most significant, in which there was a more than 20% reduction in the forecast error. To further detail the improvements in intensity, Fig. 3 shows the SLP, WIND and 48-h PP in the square region mentioned in section 3.1 at 48 h for the truth, control and OSSE runs. In the true run, the depression system occupied almost the entire region, and its lowest pressure was 1000 hPa. Strong horizontal wind (> 15 m s^{-1}) formed in a ring, and the region affected by the strong wind was mainly located in the upper right quadrant, in the shape of a crescent. In addition, the region with convective precipitation was located in the lower right corner of this square, was oriented from southeast to northwest, and had a maximum of > 35 mm for 48 h. Without dropwindsonde data, the forecast depression was a little weaker, with a minimum SLP of > 1000 hPa, and the region it controlled was a little west of the truth. Moreover, strong wind (over level 7) did not form a ring in this case, but instead extended to the south. The region affected by strong wind was distributed almost zonally. The precipitation zone was shaped like a scorpion's tail, with the main body distributed east to west. After assimilating the dropwindsonde data, the forecast depression was deeper (< 1000 hPa) and controlled almost the entire region again, indicating a trend towards the true situation. More-

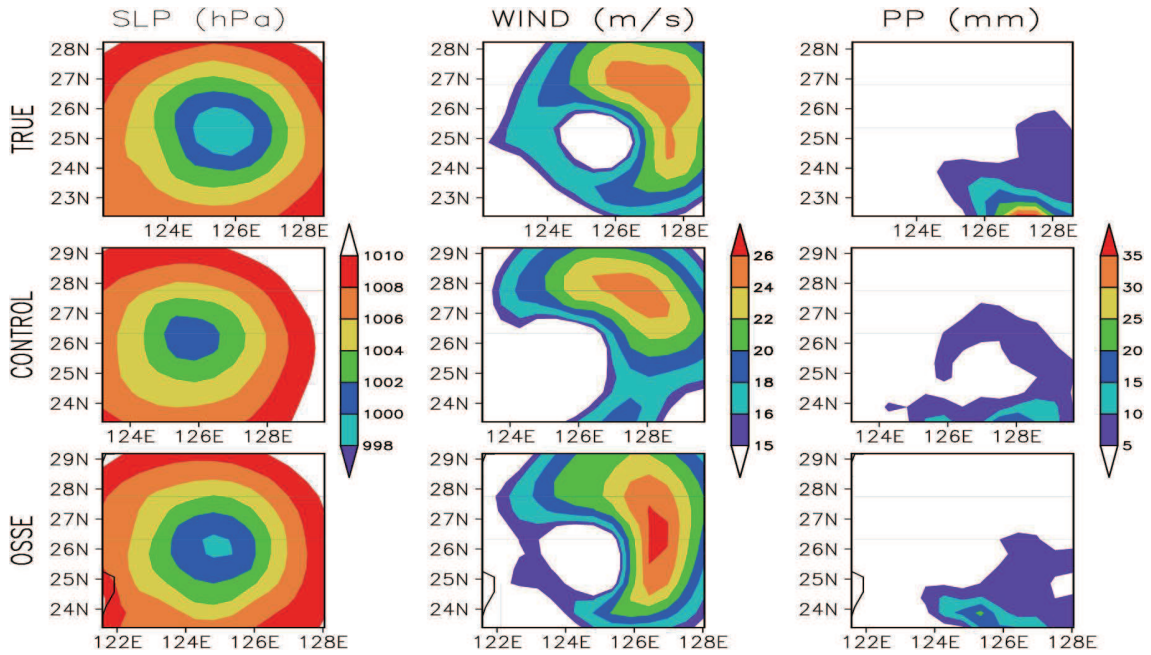

Fig. 3. SLP, horizontal wind speed (at 925 hPa) and accumulated (48-h) convective precipitation patterns in the allocated region at 48 h for the true, control and OSSE runs for case Fanapi1 (2010).

over, the region affected by strong wind encircled the eye region, as in the truth. Although the strong wind region was distributed almost meridionally, the crescent shape was pronounced. However, it should be noted that the forecast wind speed was stronger than the truth, with a maximum of > 26 m s^{-1}. The precipitation zone had a distribution similar to that for the true situation. However, the amount was much less than the truth, being < 20 mm for almost the entire region. Generally, if dropwindsondes are deployed using the CNOP sensitivity for case Fanapi1 (2010) as a guide, the improvements in the intensity forecast could be significant, relative to if the forecast is determined without dropwindsondes. The SLP, WIND and precipitation zones can be predicted toward the true situation, indicating that the CNOP sensitivity is valid in the intensity forecast.

The corresponding streamlines at 850, 500 and 200 hPa for the initial and terminal times are displayed in Fig. 4 to demonstrate the synoptic features captured by the CNOP sensitivity. At the initial time, the highest CNOP sensitivity in the lower and middle levels corresponded to the region of inflow into the TC center; in the upper level, this region was related to the outflow from the TC center. That is, the regions where mass and energy are exchanged between the storm and surrounding environment were identified as the most sensitive regions for adaptive observations. This identification was important for following the development or dissipation of this TC, which is consistent with the findings of Peng and Reynolds (2006). Hence, it is reasonable to suggest that deploying dropwindsondes in these regions would have significant benefits for both track and intensity forecasts.

The forecast errors in the form of energy [Eq. (2)] at the end of the 48-h evolution are also shown in Fig. 4. The most important part is associated with the storm, which explains why eliminating initial errors with the CNOP pattern could reduce the corresponding TC forecast errors.

We also examined in detail the case in which the greatest decrease in intensity forecast accuracy was found. Of the five cases that showed increased forecast errors after utilizing the dropwindsonde data, the intensity forecast for Malou1 (2010) was the furthest from the truth (Fig. 2). Without dropwindsondes, differences between the intensity forecasts for the control and truth runs existed at two time points (12 and 24 h), and were around 10%. During the next 24 h, the intensity forecast of the control run was the same as that of the truth run, indicating a very accurate intensity forecast prior to adaptive observation. However, after assimilating dropwindsondes, differences increased at every time interval except 12 h, with an average error of 21.77%, which was over six times that of the control run (3.40%). The error at 42 h was the largest at nearly 60%. The following detailed analysis focuses on this particular time point.

The three elements of the TC intensity index (SLP, WIND and PP) are shown in Fig. 5 for the Malou1 (2010) case at 42 h. The SLP, WIND and PP patterns were identical in the truth and control runs. All of them showed that Malou1 (2010) was a comparatively weak TC system: the central SLP was 1009.4 hPa within a narrow zone; the regions where horizontal wind speed at 925 hPa was larger than 15 m s^{-1} were concentrated in a very small range close to the right boundary; and the maximum precipitation amount was only 6 mm for a 42-h period. After assimilating the dropwindsonde data, the forecast intensity was stronger than the truth: the central SLP was below 1009.2 hPa with an expanded range; the region of strong horizontal wind was still at the right boundary, but its

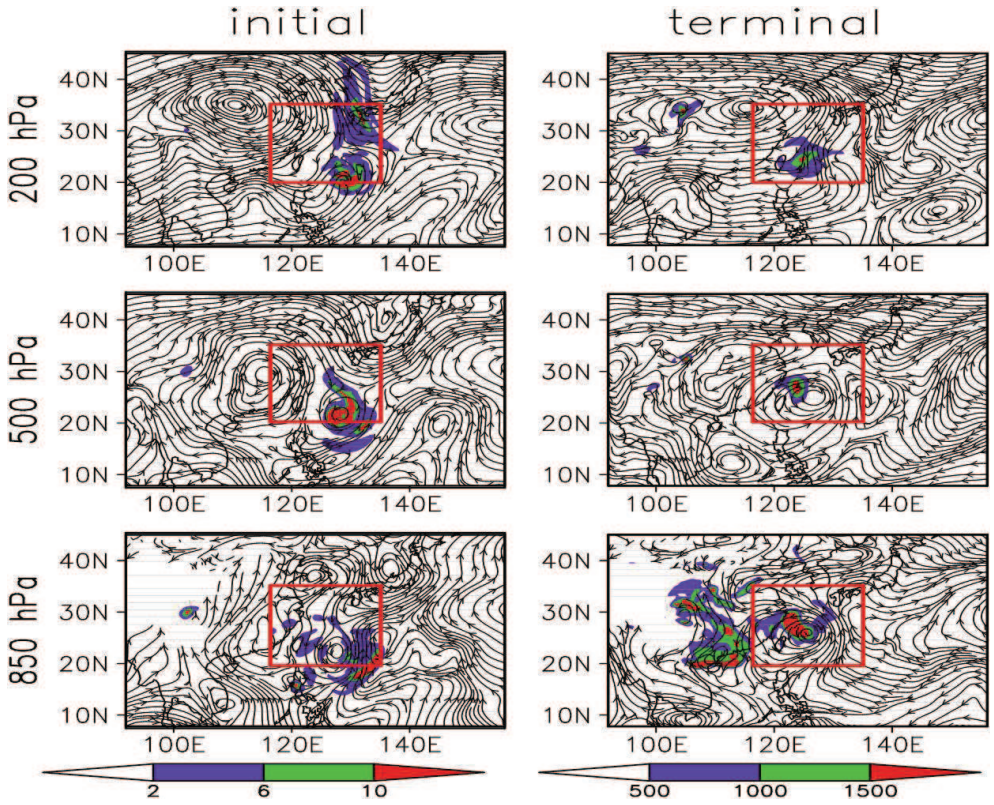

Fig. 4. Streamlines at 850, 500 and 200 hPa for the initial (0 h) and terminal (48 h) time points for the case Fanapi1 (2010). Shading shows the patterns of CNOP initial errors and forecast errors at 48 h. The red rectangle in each panel is the verification region.

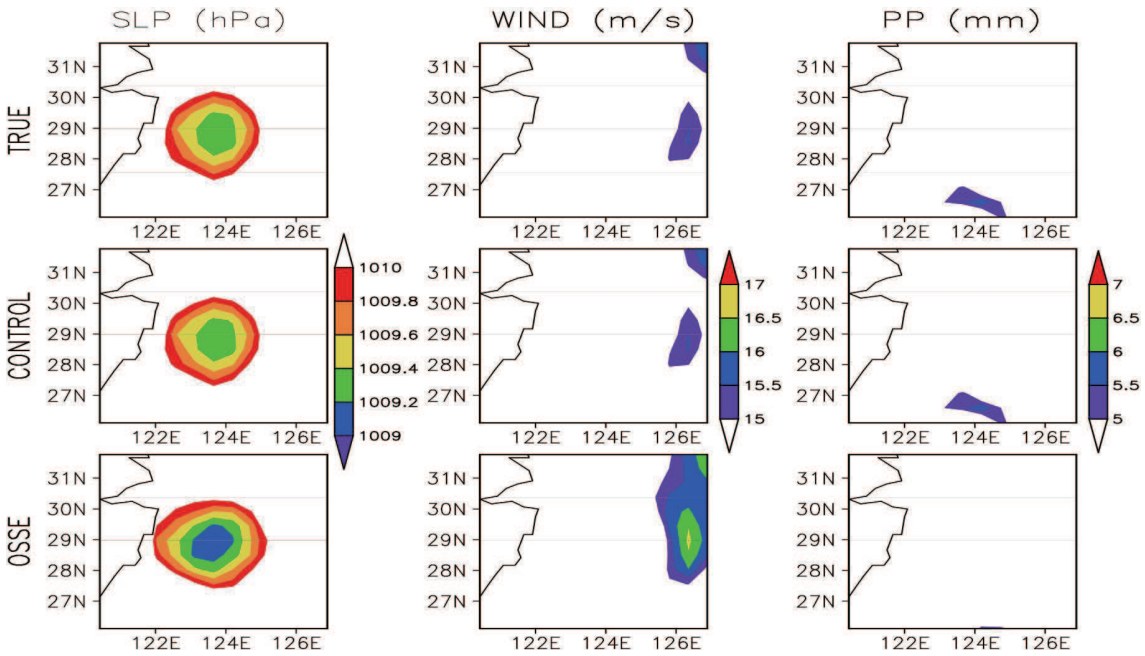

Fig. 5. The same as Fig. 3, but for the case Malou1 (2010) at 42 h.

size had doubled and the maximum was now near 17 m s^{-1}. However, the precipitation had decreased obviously in both amount and range. Of note is that the differences between the truth and OSSE runs were larger than those between the truth and control runs, as this indicates that the intensity forecast using the CNOP guided dropwindsonde data was inaccurate, relative to the forecast that used no additional data.

What is the reason for the decline in accuracy of the inten-

sity forecast? Is the sensitive region identified by the CNOP incorrect? Or are there other possibilities? To investigate the possible reasons for the deterioration in intensity forecast accuracy, streamlines for different levels at the initial and terminal times are shown in Fig. 6. Judging from the background streamlines, the TC vortex of Malou1 (2010) was a really weak system at initial time, which could only be traced to within 20°–25°N and 125°–130°E at 850 hPa. Additionally, there were both large-scale and many local systems, which comprised a really complicated environment. In detail, the strong subtropical high and mid-latitude trough separately controlled the western North Pacific for over 30° of longitude and the continent. Simultaneously, there were several local highs and lows distributed in the tropical zones. With respect to the CNOP sensitivity, it reflected different regimes at different levels. In the middle and upper levels, the sensitivity was associated with the trough. In the lower levels, it was related to the storm itself. Over the 48-h period of evolution, all of the above systems changed substantially and a more complicated environment appeared. The range of the subtropical high over the western North Pacific narrowed in both the zonal and meridional directions. The mid-latitude trough moved eastward by about 5° in longitude, and within the verification region. TC Malou1 (2010) strengthened and moved northwestward during these 48 h, forming a prominent cyclone at lower and middle levels. However, most of the forecast errors caused by CNOP pattern initial errors did not fall within the verification region at 48 h. That is to say, eliminating the initial errors with the CNOP pattern does not necessarily lead to a forecast error reduction in the verification region. According to our previous research, a high proportion of forecast errors within the verification region compared with those in the whole model region is one necessary condition to obtain marked forecast improvements by adaptive observations (Qin et al., 2013). Hence, an improvement in forecast skill was not obtained in this case. Unexpectedly, the forecast accuracy decreased instead, and the reason behind this was the complicated environment, together with a weak TC vortex. Not one of the systems within the verification region could dominate the streamlines there.

5. Discussion and conclusion

TC intensity forecasting is a complicated problem in the field of weather forecasting. The consensus is that numerical modeling needs improvement. In this context, the general positive effects of adaptive observations on TC track forecasts inspired us to investigate the impacts of additional observations on TC intensity forecasts. Depending on the outcome, it would then be possible to consider upgrading the TC intensity forecast skill from this point of view.

We defined a TC intensity index that focuses on the synthetic impacts on affected regions, which are caused by SLP, WIND and PP. This new index differs from the conventional definition by using the number of grid points satisfying certain constraints within a geographic square. The higher the

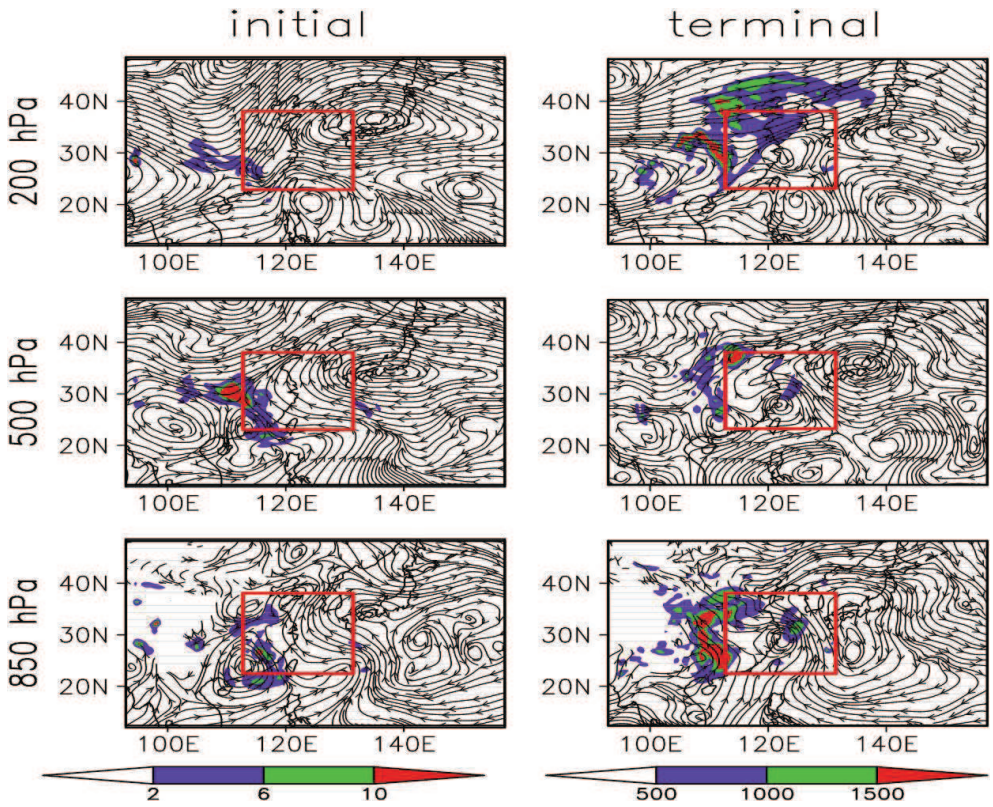

Fig. 6. The same as Fig. 4, but for the case Malou1 (2010).

index value is, the more intense the TC is.

Using this new definition of TC intensity, we estimated the impacts of the CNOP sensitivity on the intensity forecasts for 20 cases. The OSSE results for these 20 cases showed that 15 of them displayed improvements in the intensity forecast, with reductions of intensity forecast errors ranging from 0.12% to 8.59%. However, five of them showed declines in forecast accuracy ranging from 0.20% to 18.37%. According to the properties of the cases that showed improvements, the level of improvement was much more than the level of deterioration, indicating that the CNOP sensitivity generally had a positive effect on the TC intensity forecasts. Synoptic analyses of representative cases provided further details. For the case with improvement, the CNOP sensitivity captured those regions that are important for following the development or dissipation of a TC case. Therefore, with the assimilation of dropwindsonde data within the CNOP sensitivity, the patterns of SLP, horizontal wind at 925 hPa and accumulated convective precipitation moved toward the true situation, as compared with the control.

Nevertheless, the degree of improvement was not as significant as that for track forecasts (0%–51.2%) reported in Qin et al. (2013). This indicates that attempting to improve TC intensity forecasting by adaptive observations remains a challenge. Considering the interaction between atmosphere and ocean, improving numerical models (including developing optimal physical process parameterization), using higher resolutions etc., are more important than increasing observations at present for an accurate TC intensity forecast, although additional observations can quite markedly improve TC intensity forecasts in some cases. Therefore, objective evaluation of the impacts of adaptive observations on TC intensity forecasts should be made. While doing so does improve TC intensity forecasts in general terms, the degree of improvement is not significant. Nevertheless, the effects of adaptive observations are expected to be better embodied if more advanced numerical models become available.

Acknowledgements. This work was sponsored by the National Natural Science Foundation of China (Grant No. 41105040).

REFERENCES

Aberson, S. D., 2002: Two years of operational hurricane synoptic surveillance. *Wea. Forecasting*, **17**, 1101–1110.

Aberson, S. D., 2003: Targeted observations to improve operational tropical cyclone track forecast guidance. *Mon. Wea. Rev.*, **131**, 1613–1628.

Chen, B. Y., and M. Mu, 2012: The roles of spatial locations and patterns of initial errors in the uncertainties of tropical cyclone forecasts. *Adv. Atmos. Sci.*, **29**(1), 63–78, doi: 10.1007/s00376-011-0201-x.

Chen, B. Y., M. Mu, and X. H. Qin, 2013: The impact of assimilating dropwindsonde data deployed at different sites on typhoon track forecasts. *Mon. Wea. Rev.*, **141**, 2669–2682.

Chou, K. H., C. C. Wu, P. H. Lin, S. D. Aberson, M. Weissmann, F. Harnisch, and T. Nakazawa, 2011: The impact of dropwindsonde observations on typhoon track forecasts in DOTSTAR and T-PARC. *Mon. Wea. Rev.*, **139**, 1728–1743.

Duan, W. S., M. Mu, and B. Wang, 2004: Conditional nonlinear optimal perturbations as the optimal precursors for El Nino-Southern oscillation events. *J. Geophys. Res.*, **109**, D23105, doi: 10.1029/2004JD004756.

Duan, W. S., F. Xue, and M. Mu, 2009: Investigating a nonlinear characteristic of El Niño events by conditional nonlinear optimal perturbation. *Atmos. Res.*, **94**, 10–18.

Duan, W. S., and H. Y. Luo, 2010: A new strategy for solving a class of constrained nonlinear optimization problems related to weather and climate predictability. *Adv. Atmos. Sci.*, **27**, 741–749, doi: 10.1007/s00376-009-9141-0.

Elsberry, R. L., and P. A., Harr, 2008: Tropical cyclone structure (TCS08) field experiment science basis, observational platforms, and strategy. *Asia-Pacific J. Atmos. Sci.*, **44**, 209–231.

Franklin, J. L., 2009: 2008 National Hurricane Center forecast verification report. [Available online at http://www.nhc.noaa.gov/verification]

Jiang, Z. N., and D. H. Wang, 2010: A study on precursors to blocking anomalies in climatological flows by using conditional nonlinear optimal perturbations. *Quart. J. Roy. Meteor. Soc.*, **136**, 1170–1180.

Jiang, Z. N., and D. H. Wang, 2011: Conditional nonlinear optimal perturbations: Behaviour during the evolution of cold vortices over northeast China. *Quart. J. Roy. Meteor. Soc.*, **138**, 198–208.

Jiang, Z. N., M. Mu, and D. H. Wang, 2011: Optimal perturbations triggering weather regime transitions: Onset of blocking and strong zonal flow. *Adv. Atmos. Sci.*, **28**(1), 59–68, doi: 10.1007/s00376-010-9097-0.

Lin, I. I., C. C. Wu, I. F. Pun, and D. S. Ko, 2007: Upper-ocean thermal structure and the Western North Pacific category 5 typhoons. Part I: Ocean features and the category 5 typhoons' intensification. *Mon. Wea. Rev.*, **136**, 3288–3306.

Lin, I. I., I. F. Pun, and C. C. Wu, 2008: Upper-ocean thermal structure and the Western North Pacific category 5 typhoons. Part II: Dependence on translation speed. *Mon. Wea. Rev.*, **137**, 3744–3757.

Mu, M., and Z. Y. Zhang, 2006: Conditional nonlinear optimal perturbations of a two-dimensional quasigeostrophic model. *J. Atmos. Sci.*, **63**, 1587–1604.

Mu, M., and Z. N. Jiang, 2011: Similarities between optimal precursors that trigger the onset of blocking events and optimally growing initial errors in onset prediction. *J. Atmos. Sci.*, **68**, 2860–2877, doi: 10.1175/JAS-D-11-037.1.

Mu, M., W. S. Duan, and B. Wang, 2003: Conditional nonlinear optimal perturbation and its applications. *Nonlinear Processes in Geophysics*, **10**, 493–501.

Mu, M., L. Sun, and H. A. Dijkstra, 2004: The sensitivity and stability of the ocean's thermohaline circulation to finite-Amplitude perturbations. *J. Phys. Oceanogr.*, **34**, 2305–2315.

Mu, M., Duan, W. S., and Wang, B., 2007: Season-dependent dynamics of nonlinear optimal error growth and ENSO predictability in a theoretical model. *J. Geophys. Res.*, **112** , D10113, doi: 10.1029/2005JD006981.

Mu, M., F. F. Zhou, and H. L. Wang, 2009: A method for identifying the sensitive areas in targeted observations for tropical cyclone prediction: Conditional nonlinear optimal perturbation. *Mon. Wea. Rev.*, **137**, 1623–1639.

Palmer, T. N., R. Gelaro, J. Barkmeijer, and R. Buizza, 1998: Singular vectors, metrics, and adaptive observations. *J. Atmos. Sci.*, **55**, 633–653.

Peng, M. S., and C. A. Reynolds, 2006: Sensitivity of tropical cyclone forecasts as revealed by singular vectors. *J. Atmos. Sci.*, **63**, 2508–2528.

Qin, X. H., and M. Mu, 2011a: A study on the reduction of forecast error variance by three adaptive observation approaches for tropical cyclone prediction. *Mon. Wea. Rev.*, **139**, 2218–2232.

Qin, X. H., and M. Mu, 2011b: Influence of conditional nonlinear optimal perturbations sensitivity on typhoon track forecasts. *Quart. J. Roy. Meteor. Soc.*, **138**, 185–197.

Qin, X. H., W. S. Duan, and M. Mu, 2013: Conditions under which CNOP sensitivity is valid for tropical cyclone adaptive observations. *Quart. J. Roy. Meteor. Soc.*, **139**, 1544–1554.

Sun, G. D., and M. Mu, 2009: Nonlinear feature of the abrupt transitions between multiple equilibria states of an ecosystem model. *Adv. Atmos. Sci.*, **26**(2), 293–304, doi: 10.1007/s00376-009-0293-8.

Sun, G. D., and M. Mu, 2011: Response of a grassland ecosystem to climate change in a theoretical model. *Adv. Atmos. Sci.*, **28**(6), 1266–1278, doi: 10.1007/s00376-011-0169-6.

Sun, G. D., and M. Mu, 2012: Inducing unstable grassland equilibrium states due to nonlinear optimal patterns of initial and parameter perturbations: Theoretical models. *Adv. Atmos. Sci.*, **29**(1), 79–90, doi: 10.1007/s00376-011-0226-1.

Sun, L., M. Mu, D. J. Sun, and X. Y. Yin, 2005: Passive mechanism of decadal variation of thermohaline circulation. *J. Geophys. Res.*, **110**, C07025, doi: 10.1029/2005JC002897.

Sun, G. D., M. Mu, and Y. L. Zhang, 2010: Algorithm studies on how to obtain a conditional nonlinear optimal perturbation (CNOP). *Adv. Atmos. Sci.*, **27**(6), 1311–1321, doi: 10.1007/s00376-010-9088-1.

Wang, B., and X. W. Tan, 2009: A fast algorithm for solving CNOP and associated target observation tests. *Acta Meteorologica Sinica*, **23**(4), 387–402.

Wang, H. L., M. Mu, and X. Y. Huang, 2011: Application of conditional non-linear optimal perturbations to tropical cyclone adaptive observation using the Weather Research Forecasting (WRF) model. *Tellus*, **63**, 939–957.

Wang, Y. Q., and H. J. Cheng, 2008: A numerical investigation of the eyewall evolution in a Landfalling typhoon. *Mon. Wea. Rev.*, **137**, 21–40.

Weng, Y. H., and F. Q. Zhang, 2012: Assimilating airborne doppler radar observations with an ensemble kalman filter for convection-permitting hurricane initialization and prediction: Katrina (2005). *Mon. Wea. Rev.*, **140**, 841–859.

Wu, C. C., and Coauthors, 2005: Dropwindsonde observations for typhoon surveillance near the Taiwan region (DOSTAR): An overview. *Bull. Amer. Meteor. Soc.*, **86**, 787–790.

Wu, C. C., K. H. Chou, P. H. Lin, S. D. Aberson, M. S. Peng, and T. Nakazawa, 2007: The impact of dropwindsonde data on typhoon track forecasts in DOTSTAR. *Wea. Forecasting*, **22**, 1157–1176.

Wu, C. C., Y. H. Huang, and G. Y. Lien, 2011: Concentric eyewall formation in typhoon Sinlaku (2008). Part I: Assimilation of T-PARC data based on the Ensemble Kalman Filter (EnKF). *Mon. Wea. Rev.*, **140**, 506–527.

Xu, J., and Y. Q., Wang, 2010: Sensitivity of the simulated tropical cyclone inner-core size to the initial vortex size. *Mon. Wea. Rev.*, **138**, 4135–4157.

Yu, Y. S., W. S. Duan, H. Xu, and M. Mu, 2009: Dynamics of nonlinear error growth and season-dependent predictability of El Niño events in the Zebiak-Cane model. *Quart. J. Roy. Meteor. Soc.*, **135**, 2146–2160.

Yu, Y. S., M. Mu, and W. S. Duan, 2012a: Does model parameter error cause a significant "spring predictability barrier" for El Niño events in the Zebiak-Cane model? *J. Climate*, **25**(4), 1263–1277.

Yu, Y. S., M. Mu, W. S. Duan, and T. T. Gong, 2012b: Contribution of the location and spatial pattern of initial error to uncertainties in El Niño predictions. *J. Geophys. Res.*, **117**, doi: 10.1029/2011JC007758.

Zeng, Z. H., Y. Q. Wang, and C. C. Wu, 2006: Environmental dynamical control of tropical cyclone intensity—An observational study. *Mon. Wea. Rev.*, **135**, 38–59.

Zhou, F. F., and M. Mu, 2011: The impact of verification area design on tropical cyclone targeted observations based on the CNOP method. *Adv. Atmos. Sci.*, **28**(5), 997–1010, doi: 10.1007/s00376-011-1003-x.

Zhou, F. F., and M. Mu, 2012a: The impact of horizontal resolution on the CNOP and on its identified sensitive areas for tropical cyclone predictions. *Adv. Atmos. Sci.*, **29**(1), 36–46, doi: 10.1007/s00376-012-1174-0.

Zhou, F. F., and M. Mu, 2012b: The time and regime dependencies of sensitive areas for tropical cyclone prediction using the CNOP method. *Adv. Atmos. Sci.*, **29**(4), 705–716, doi: 10.1175/MWR3278.1.